Protein Science (1998), 7:556–563. Cambridge University Press. Printed in the USA.

Structures of murine carbonic anhydrase IV and human carbonic anhydrase II complexed with brinzolamide: Molecular basis of isozyme-drug discrimination

TRAVIS STAMS,[1] YUN CHEN,[1] P. ANN BORIACK-SJODIN,[1,4] JONATHAN D. HURT,[2] JOHN LIAO,[3] JESSE A. MAY,[3] TOM DEAN,[3] PHILIP LAIPIS,[2] DAVID N. SILVERMAN,[2] AND DAVID W. CHRISTIANSON[1]

[1]Roy and Diana Vagelos Laboratories, Department of Chemistry, University of Pennsylvania, Philadelphia, Pennsylvania 19104-6323
[2]Department of Biochemistry and Molecular Biology, University of Florida College of Medicine, Gainesville, Florida 32610-0267
[3]Alcon Laboratories, Inc., 6201 South Freeway, Fort Worth, Texas 76134-2099

(RECEIVED November 3, 1997; ACCEPTED December 18, 1997)

Abstract

Carbonic anhydrase IV (CAIV) is a membrane-associated enzyme anchored to plasma membrane surfaces by a phosphatidylinositol glycan linkage. We have determined the 2.8-Å resolution crystal structure of a truncated, soluble form of recombinant murine CAIV. We have also determined the structure of its complex with a drug used for glaucoma therapy, the sulfonamide inhibitor brinzolamide (Azopt™). The overall structure of murine CAIV is generally similar to that of human CAIV; however, some local structural differences are found in the active site resulting from amino acid sequence differences in the "130's segment" and the residue-63 loop (these may affect the nearby catalytic proton shuttle, His-64). Similar to human CAIV, the C-terminus of murine CAIV is surrounded by a substantial electropositive surface potential that may stabilize the interaction with the phospholipid membrane. Binding interactions observed for brinzolamide rationalize the generally weaker affinity of inhibitors used in glaucoma therapy toward CAIV compared with CAII.

Keywords: brinzolamide; carbonic anhydrase; crystallography

A family of seven well-characterized isozymes designated I–VII, the mammalian carbonic anhydrases (CAs) catalyze the reversible hydration of carbon dioxide through a two-step, zinc–hydroxide mechanism (Silverman & Lindskog, 1988; Sly & Hu, 1995; Christianson & Fierke, 1996; Stams & Christianson, 1998).

$$Zn\text{-}OH^- + CO_2 + H_2O \leftrightarrow Zn\text{-}H_2O + HCO_3^-.$$

$$Zn\text{-}H_2O \leftrightarrow Zn\text{-}OH^- + H^+.$$

The three-dimensional structures of human CAI (Kannan et al., 1984), human CAII (Liljas et al., 1972; Håkansson et al., 1992), bovine CAII (Eriksson & Liljas, 1993), human CAIV (Stams et al., 1996), and murine CAV (Boriack-Sjodin et al., 1995) reveal a common fold dominated by a β-sheet superstructure. The catalytically obligatory zinc ion resides on one face of the β-sheet at the bottom of a 15-Å deep active site cavity. Zinc is liganded by His-94, His-96, His-119, and hydroxide ion with tetrahedral geometry; Thr-199 accepts a hydrogen bond from zinc-bound hydroxide ion. In isozymes II and IV, His-64 acts as a catalytic proton shuttle between zinc-bound solvent and bulk solvent.

One of the most efficient carbonic anhydrase isozymes (Baird et al., 1997), CAIV is membrane-associated (Sly & Hu, 1995; Stams & Christianson, 1998). On the plasma membrane of specific segments of kidney tubules, CAIV plays important roles in modulating equilibrium pH in the lumen and in bicarbonate reabsorption (Lucci et al., 1983; Brown et al., 1990; Brechue et al., 1991); in lung, CAIV functions to catalyze the dehydration of serum bicarbonate to CO_2 (Effros et al., 1981; Fleming et al., 1993). In the eye, CAIV is located in the endothelial cells of the choriocapillaris (Hageman et al., 1991), and there is functional evidence for its localization in the basolateral membranes of nonpigmented epithelium in ciliary processes (Hageman et al., 1991). This implicates CAIV as a possible pharmaceutical target for glaucoma therapy: topically applied CA inhibitors are known to significantly decrease intraocular pressure, a major risk factor of glaucoma.

Reprint requests to: D.W. Christianson, Roy and Diana Vagelos Laboratories, Department of Chemistry, University of Pennsylvania, Philadelphia, Pennsylvania 19104-6323; e-mail: chris@xtal.chem.upenn.edu.
[4]Present address: Laboratory of Molecular Biophysics, The Rockfeller University, 1230 York Avenue, New York, New York 10021.

Recently, the crystal structure of human CAIV has been determined (Stams et al., 1996). The zinc binding site and the hydrophobic substrate binding pocket of CAIV are generally similar to those of CAII. However, several differences are found between these two isozymes. CAIV contains two disulfide linkages, Cys-6–Cys-11G and Cys-23–Cys-203, that are not conserved in CAII. Not only do these linkages stabilize the conformation of the N-terminal domain, but the disulfide Cys-23–Cys-203 stabilizes an active site loop containing a *cis*-peptide linkage between Pro-201 and Thr-202. Another intriguing difference is found in the loop containing the catalytic proton shuttle, His-64. In most mammalian carbonic anhydrases, the adjacent residue at position 63 is glycine. Rodent CAIVs are exceptional in that Gly-63 is replaced by glutamine, and this difference largely explains the apparently impaired proton transfer and catalysis by rodent CAIVs (Tamai et al., 1996).

A notable difference between human CAIV and other isozymes is that the Val-131–Asp-136 segment adopts an extended loop conformation instead of an α-helix conformation as found in CAII. Furthermore, the disordering of the Lys-124–Glu-138 region in one of two molecules of human CAIV in the asymmetric unit may result from the substantial cleavage of the Arg-129–Asn-130 linkage (Stams et al., 1996). Because this region of the active site is known to be a critical affinity determinant for inhibitor binding (Baldwin et al., 1989), the complex of CAIV with a sulfonamide inhibitor may reveal important structural features relevant to the design of drugs used to treat glaucoma.

Here, we report the 2.8-Å resolution X-ray crystal structure of a truncated, secretory form of murine CAIV produced in *Escherichia coli* (Okuyama et al., 1992, 1995). The truncated form lacks the C-terminal glycosylphosphatidylinositol (GPI) anchor, but appears to have full activity (Hurt et al., 1997). Recombinant CAIV contains 264 residues, with 57% sequence identity to human CAIV and 33% sequence identity to human CAII (identities based on alignment of tertiary structures). The maximal value of k_{cat}/K_m for CO_2 hydration exhibited by murine CAIV is 3×10^7 M^{-1} s^{-1}, threefold less than the corresponding value for human CAII or human CAIV; $k_{cat} \approx 1.0 \times 10^5$ s^{-1} at pH 7–8, which is 10-fold less than that of human CAIV (Hurt et al., 1997). Because k_{cat} reflects proton transfer from zinc-bound water to His-64 in the second step of catalysis (Silverman & Lindskog, 1988), the structure of murine CAIV and its comparison with human CAIV reveals clues regarding the molecular basis of impaired proton transfer in murine CAIV. In addition, we report the crystal structures of the CAIV–brinzolamide and CAII–brinzolamide complexes at 2.8 Å and 2.25 Å resolution, respectively, which illuminate for the first time the structural basis of drug–isozyme discrimination between CAIV and CAII.

Results and discussion

Structure of murine CAIV

The overall fold of murine CAIV is similar to that of human isozymes II and IV (Fig. 1). However, some significant differences in local active site structure may correlate with differences in catalytic activity among these three isozymes. The principal difference is found in the "130′s segment," which comprises one wall of the active site cavity about 6–8 Å away from zinc. In human CAII, this segment is a three-turn α-helix (Liljas et al., 1972; Håkansson et al., 1992). In the crystal structure of human CAIV,

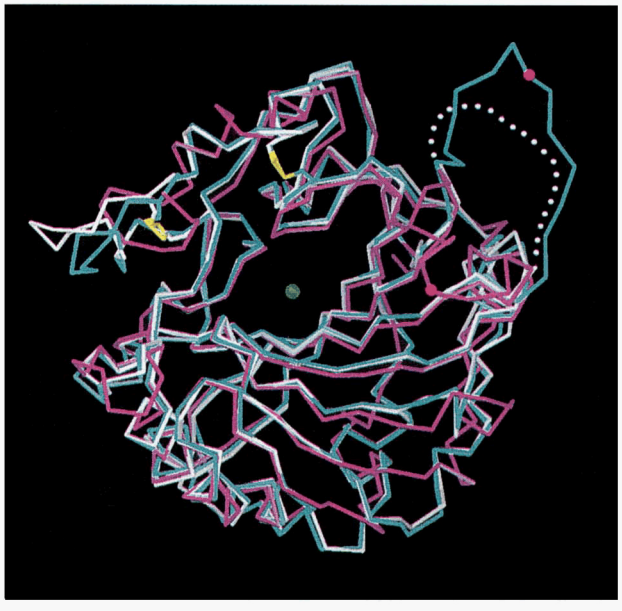

Fig. 1. Cα superposition of murine CAIV (white), human CAIV (cyan), and human CAII (magenta). The disulfide linkages of murine CAIV and human CAIV are yellow, and the active site zinc ion is green. The 130′s segment is highlighted by a red ball at position 131 in human CAII and human CAIV; electron density is not observed for this segment in murine CAIV and presumed disordered (dotted line).

there are two molecules in the asymmetric unit; in one molecule, the 130′s segment adopts an extended loop conformation, and in the second molecule, this segment is disordered due to proteolytic nicking at the Arg-129–Asn-130 linkage (Stams et al., 1996). This segment is similarly disordered in murine CAIV, despite four- and six-amino acid deletions in the alignment with human CAII and CAIV, respectively:

```
          120         130         140
hCAII   LVHWNT--KYGDFGKAVQQPDG
mCAIV   IVHKKLTSS----KE--DSKDK
hCAIV   IVHEKEKGTSRNVKEAQDPEDE
```

Gel electrophoresis experiments with murine CAIV show no evidence of proteolytic cleavage (data not shown). Therefore, the lack of electron density for this segment indicates that the flexibility and disorder of the 130′s segment is not dependent on proteolytic nicking. Instead, it must be an inherently flexible loop in this particular isozyme.

Other structural differences among human CAII, human CAIV, and murine CAIV are found in the vicinity of the catalytic proton shuttle, His-64 (Fig. 2). In native CAII, His-64 is oriented toward the active site at pH 8.5 (the "in" conformation) (Håkansson et al., 1992); at lower pH values, His-64 rotates away from the active site to the "out" conformation (Nair & Christianson, 1991). In human CAIV, His-64 adopts the "out" conformation at pH 5.1, which appears to be consistent with the behavior of this residue in CAII. However, in murine CAIV, His-64 adopts the "out" conformation at pH 7, which contrasts with the pH-dependent conformation of

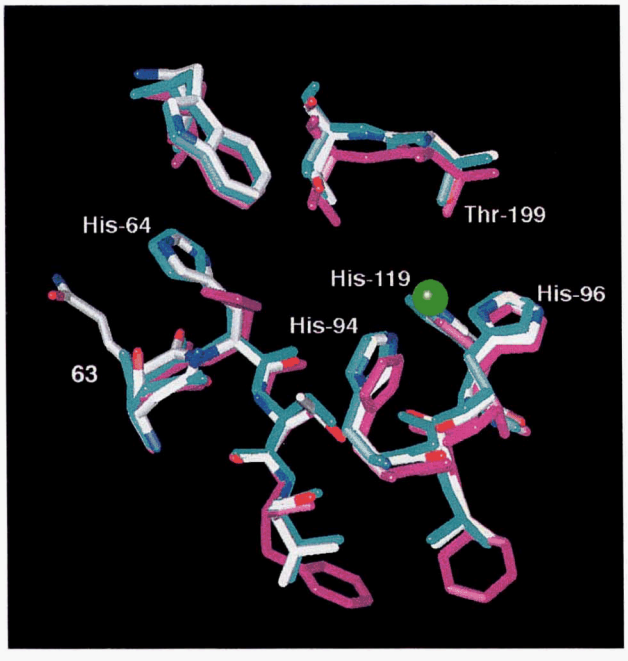

Fig. 2. Superposition of His-64 regions of murine CAIV (color coded by atom), human CAIV (cyan), and human CAII (magenta). In murine CAIV and human CAIV, His-64 occupies the "out" conformation (i.e., oriented away from the active site), whereas in human CAII, it occupies the "in" conformation (i.e., oriented toward the active site). Note that, despite the appearance of Gln-63 in murine CAIV and Gly-63 in human CAIV and human CAII, the backbone conformation of residue-63 is similar in all three structures.

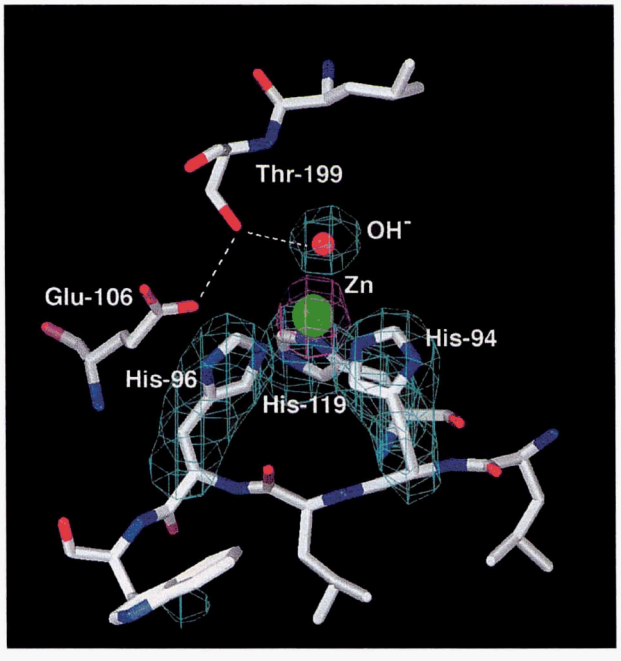

Fig. 3. Difference electron density maps of the zinc binding site of murine CAIV, generated with Fourier coefficients $|F_o| - |F_c|$ and phases calculated from the final model minus zinc (magenta, contoured at 10σ), or zinc ligands His-94, His-96, His-119, and hydroxide (cyan, contoured at 3σ). Metal coordination geometry is tetrahedral. The hydrogen bond network between zinc-bound hydroxide, Thr-199, and Glu-106 is indicated by dashed lines.

this residue in the other two isozymes. Intriguingly, the adjacent glycine residue at position 63, which is conserved among nearly all characterized carbonic anhydrases, is replaced by glutamine in murine and rat CAIVs (Tamai et al., 1996). Consequently, Gln-63 may affect the conformation and chemistry of neighboring His-64, because the k_{cat} value of murine CAIV in the pH range of 6–8 is found to be approximately 10-fold less than that of human CAIV (Baird et al., 1997; Hurt et al., 1997). These observations agree with and extend those of Tamai et al. (1996), who also provide evidence that Gln-63 → Gly substitution in murine CAIV increases the activity of the enzyme, demonstrating that Gln-63 does indeed modulate proton transfer at His-64 (Tamai et al., 1996). However, comparison of the His-64 region of human CAII, human CAIV, and murine CAIV reveals no major conformational differences in the polypeptide backbone (Fig. 2). Possibly, interactions between the side chains of Gln-63 and His-64 may modulate the function of His-64. Further enzymological and X-ray crystallographic experiments are necessary to address this speculation.

Other features in the active site of murine CAIV are similar to those of many other mammalian carbonic anhydrases (Liljas et al., 1972; Kannan et al., 1984; Håkansson et al., 1992; Eriksson & Liljas, 1993): Conserved zinc ligands are His-94, His-96, His-119, and hydroxide ion [at pH 5.1 in human CAIV, the nonprotein ligand is sulfate (Stams et al., 1996)]. An electron density map of the zinc binding site is found in Figure 3. Thr-199 accepts a hydrogen bond from zinc-bound hydroxide and orients the nucleophile for catalysis. The zinc-binding site is also stabilized by conserved "indirect" zinc ligands, i.e., residues that hydrogen bond to histidine metal ligands. Indirect ligands in the active site make the following hydrogen bonds: Nδ1 of His-94 to Oε1 of Gln-92, Nδ1 of His-96 to O of Asn-244, and Nε2 of His-119 to Oε2 of Glu-117.

Finally, the two disulfide linkages observed in human CAIV are conserved in murine CAIV. These structural elements contribute to the stabilization of CAIV against solubilization in 5% SDS (Whitney & Briggle, 1982; Waheed et al., 1996), and both disulfides are found adjacent to the enzyme active site cavity in the N-terminal region: Cys-6–Cys-11G and Cys-23–Cys-203. As found in the structure of human CAIV (Stams et al., 1996), the latter disulfide linkage apparently helps to stabilize a *cis*-peptide linkage between Pro-201 and Asn-202.

Membrane association

The biological requirement for enhanced stability of CAIV probably arises from its location in harsh, extracellular environments. As mentioned in the introduction, CAIV is a GPI-anchored membrane protein expressed on the plasma membrane of specific epithelial and endothelial cells. The GPI anchor is attached to the C-terminus of the protein (Zhu & Sly, 1990), which is located on the opposite side of the molecule relative to the active site cavity. With this geometry, the active site is oriented toward the lumen and is fully accessible for catalysis when the GPI anchor is inserted into the membrane (Stams et al., 1996).

As found for human CAIV (Stams et al., 1996), there is a significant electropositive surface potential flanking the C-terminus of murine CAIV (Fig. 4). This surface is generated by the positively charged side chains of several basic residues: Arg-37, Lys-39,

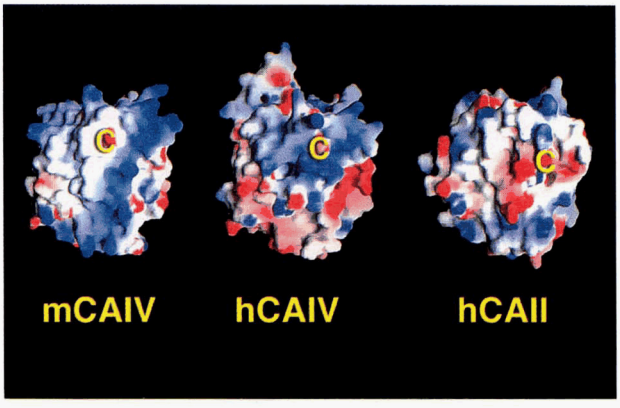

Fig. 4. Electrostatic surface potential of murine CAIV, human CAIV, and human CAII calculated with GRASP (Honig & Nicholls, 1995); the color scale ranges from $-8kT$ (red) to $+8kT$ (blue). Note the extensive positive electrostatic surface potential (blue) surrounding the C termini of murine CAIV and human CAIV (the location of each C terminus is indicated by a yellow "C"). This feature facilitates membrane adsorption and orients the enzyme active site away from the membrane so it is fully accessible for catalysis.

Arg-112, Lys-152, Lys-155, Lys-188, Lys-213, Lys-217, Lys-253, and Lys-258. Although only Lys-39, Lys-188, and Lys-258 are conserved between murine CAIV and human CAIV, the net positive surface potential *is* conserved because human CAIV has a total of 11 basic residues flanking its C-terminus (Stams et al., 1996) (Fig. 4). Except for Lys-213, these residues are not conserved in CAII (Fig. 4). This supports the proposal that these residues facilitate the interaction of CAIV with the negatively charged phosphate groups of the phospholipid membrane, and a complementary electrostatic interaction with the protein surface helps stabilize the orientation of the protein on the membrane surface (Stams et al., 1996).

Other membrane-associated proteins are known to contain clusters of basic residues that facilitate membrane adsorption; such clusters generally flank a hydrophobic myristoyl or farnesyl group that anchors the protein to the membrane surface. Experimental and theoretical analysis of basic peptide association with membranes containing acidic lipids suggests that each basic residue on the protein contributes about 1 kcal/mol to the membrane association energy under physiological conditions (Ben-Tal et al., 1996). This may explain why an equivalent number of basic residues flank the GPI-anchored C-termini of murine CAIV and human CAIV, even though these basic residues are not conserved at identical locations in primary structure.

Binding of brinzolamide (Azopt™) to CAII and CAIV

Compounds bearing sulfonamide groups have long been known to be potent inhibitors of the carbonic anhydrases (Mann & Keilin, 1940), and the most notable clinical significance of acetazolamide and related sulfonamides is in glaucoma therapy (Maren, 1984, 1987; Baldwin et al., 1989; Greer et al., 1994). Inhibition of ocular carbonic anhydrase decreases aqueous humor secretion, which in turn lowers intraocular pressure: this is the major risk factor of primary open-angle glaucoma (Quigley, 1993; Tielsch et al., 1994). Although isozyme II is presumed to be the predominant ocular receptor of topically applied sulfonamide inhibitors, the localization of isozyme IV in certain ocular tissues (Hageman et al., 1991) also implicates this isozyme (Maren et al., 1993). Notably, the affinity of CAIV for sulfonamide inhibitors is up to 100-fold less than that of CAII, suggesting that the rational design of isozyme-specific inhibitors would be possible once the molecular basis for this phenomenon is understood (Baird et al., 1997).

Brinzolamide (Azopt™) is a potent sulfonamide inhibitor of the carbonic anhydrases, with IC_{50} values of 3.2 nM and 45.3 nM against CAII and CAIV, respectively (Camras et al., 1997; Dean et al., 1997; Shin et al., 1997; Stewart et al., 1997) (Fig. 5). This is the newest carbonic anhydrase inhibitor approved for use in the treatment of glaucoma. Comparison of the CAII–brinzolamide and CAIV–brinzolamide complexes reveals significant structural differences accounting for the generally decreased affinity of sulfonamide inhibitors toward isozyme IV.

Brinzolamide binding to the active site zinc ion of CAII is similar to that observed in other CAII–sulfonamide structures (Eriksson et al., 1986, 1988; Baldwin et al., 1989; Vidgren et al., 1990; Prugh et al., 1991; Cappalonga et al., 1992), and an electron density map is found in Figure 6. The ionized sulfonamide nitrogen coordinates to zinc and displaces zinc-bound hydroxide. In addition, this nitrogen donates a hydrogen bond to the hydroxyl group of Thr-199, which in turn donates a hydrogen bond to the carboxylate group of Glu-106. Sulfonamide oxygen O_3 displaces the "deep" water molecule located at the mouth of the hydrophobic pocket (Eriksson et al., 1986, 1988). This oxygen also accepts a hydrogen bond from the backbone amide NH of Thr-199. Sulfonamide oxygen O_4 is not within hydrogen bonding distance of any hydrogen bond donors, nor is it within the inner sphere of zinc coordination (Zn^{+2}-O separation = 3.9 Å).

The oxygen atoms of the *endo*-sulfonamide group, designated O_2 and O_5, make polar interactions with active site residues: O_5 accepts hydrogen bonds from the ϵNH_2 of Gln-92 and a solvent molecule, and O_2 engages in a weakly polar, dipole–quadrupole interaction with C_3-H of Phe-131. Finally, the aliphatic ether "tail" of brinzolamide makes extensive van der Waals contacts with hydrophobic residues on one wall of the active site cavity (Leu-198, Pro-202) and also on the opposite wall (Phe-131 and Val-135 in the 130′s segment).

The conformation of the six-membered sulfonamide ring of brinzolamide is such that the ethylamine group adopts a pseudo-equatorial conformation. This allows the ethylamine nitrogen to hydrogen bond with the hydroxyl group of Thr-200. The ethylamine group sterically forces proton shuttle group His-64 from the native, "in" conformation (i.e., pointing toward the active site) to

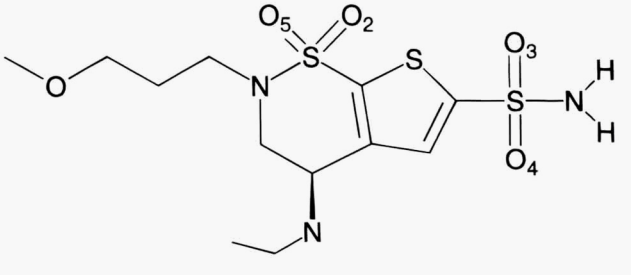

Fig. 5. Brinzolamide (Azopt™; (+)-4-ethylamino-3,4-dihydro-2-(3-methoxy)propyl-2H-thieno[3,2-e]-1,2-thiazine-6-sulfonamide-1,1-dioxide) is a potent CA inhibitor with IC_{50} values of 3.2 nM and 45 nM against CAII and CAIV, respectively.

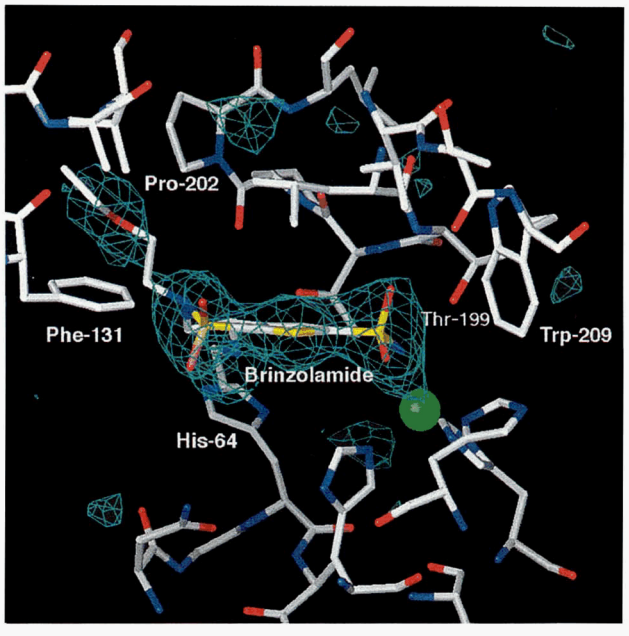

Fig. 6. Difference electron density map of the human CAII–brinzolamide complex, generated with Fourier coefficients $|F_o| - |F_c|$ and phases calculated from the final model minus the atoms of brinzolamide (contoured at 3σ). The sulfonamide nitrogen of brinzolamide coordinates to zinc and displaces zinc-bound hydroxide, thereby maintaining tetrahedral metal coordination geometry. The aliphatic tail of brinzolamide makes van der Waals contact with Phe-131 and Pro-202.

the "out" conformation (i.e., pointing away from the active site), a phenomenon that has been observed in the binding of related inhibitors and is thought to contribute a factor of ~5 to affinity due to the resultant displacement of ordered solvent (Baldwin et al., 1989; Smith et al., 1994).

The electron density map of the CAIV–brinzolamide complex reveals that the inhibitor binds to the active site zinc ion in a manner generally similar to that observed in the CAII–brinzolamide complex (data not shown): (1) an ionized sulfonamide nitrogen displaces zinc-bound hydroxide and donates a hydrogen bond to Thr-199; (2) the backbone NH group of Thr-199 donates a hydrogen bond to one sulfonamide oxygen; (3) Thr-200 accepts a hydrogen bond from N1 of the inhibitor; and (4) the ϵNH_2 group of Gln-92 donates a hydrogen bond to O_5 of the inhibitor. However, brinzolamide makes three intermolecular contacts with CAII that are *not* found in the CAIV complex. These include: (1) a dipole–quadrupole interaction between the inhibitor O_2 atom and the C_3-H of Phe-131; (2) a hydrogen bond between the inhibitor O_5 atom and a solvent molecule; and (3) extensive van der Waals contacts between the aliphatic ether "tail" of the inhibitor and (a) the Pro-202 region of the hydrophobic wall in the active site, and (b) residues Phe-131 and Val-135 of the 130′s segment. A superposition of the two enzyme active sites is found in Figure 7, and the overall enzyme structures are compared in Figure 8. In the CAIV–brinzolamide complex, the 130′s segment remains disordered, and

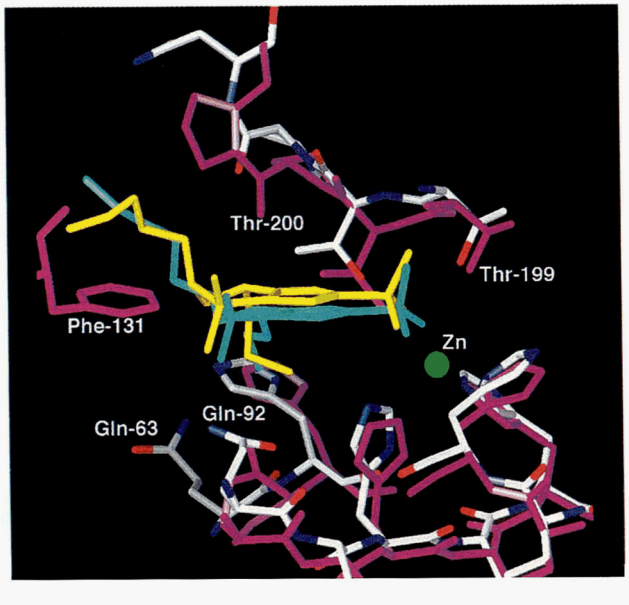

Fig. 7. Superposition of murine CAIV– (color coded by atom) and human CAII (magenta)–brinzolamide (yellow in murine CAIV; green in human CAII) complexes. Note the similarity in binding except for the loss of hydrophobic interaction between the tail of brinzolamide and residues Phe-131 and Pro-202 in murine CAIV.

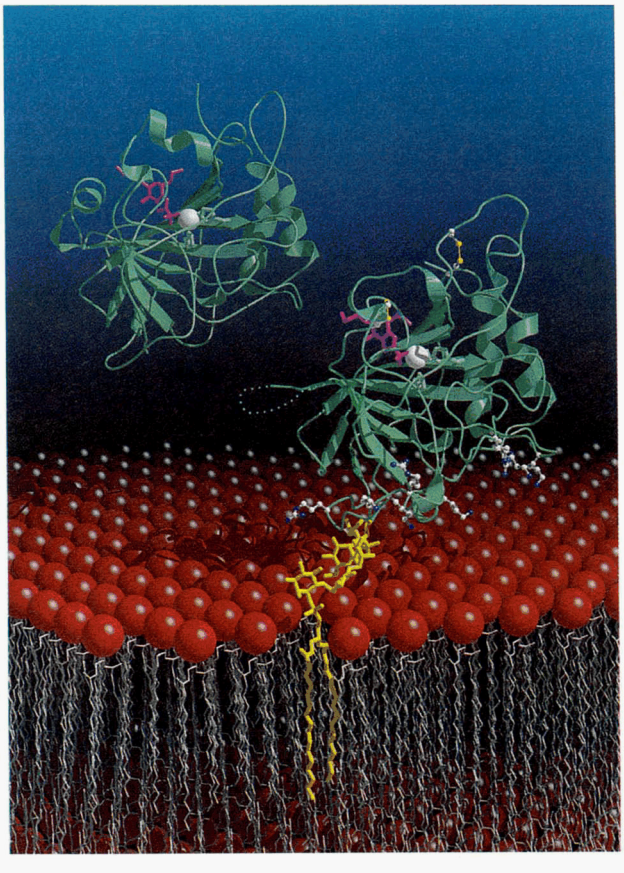

Fig. 8. CAII–brinzolamide and CAIV–brinzolamide complexes (upper left and lower right, respectively). Brinzolamide is magenta; the CAIV–membrane interaction is represented schematically, where the GPI anchor (yellow) attached to the C-terminus of the enzyme is inserted into the phospholipid bilayer. Basic residues flanking the GPI anchor stabilize the CAIV orientation by interacting with negatively charged phosphates (red). Figure prepared with MOLSCRIPT (Kraulis, 1991) and Raster 3D (Bacon & Anderson, 1988; Merritt & Murphy, 1994).

Table 1. *Data collection and refinement statistics*

	Native murine CAIV	Murine CAIV–brinzolamide	Human CAII–brinzolamide
Number of measured reflections	26,921	24,955	18,107
Number of unique reflections	6,750	7,084	8,703
Maximum resolution (Å)	2.8	2.8	2.25
R_{merge}[a]	0.083	0.097	0.098
Completeness of data (%)	94.8	97.9	65.5
Number of reflections used in refinement ($>2\sigma$)	5,404	5,789	7,483
Number of reflections in R_{free} test set	664	717	—
R_{cryst}[b]	0.182	0.191	0.144
R_{free}[c]	0.267	0.277	—
Number of non-hydrogen atoms[d]	2,019	2,045	2,064
Number of solvent molecules included in refinement	9	3	55
RMSD from ideal bond lengths (Å)	0.007	0.007	0.013
RMSD from ideal bond angles (°)	1.4	1.4	3.0
RMSD from ideal dihedral angles (°)	25.2	25.6	26.2
RMSD from ideal improper angles (°)	1.2	1.1	1.2

[a] R_{merge} for replicate reflections, $R = \Sigma|I_h - \langle I_h\rangle|/\Sigma\langle I_h\rangle$; I_h = intensity measured for reflection h; $\langle I_h\rangle$ = average intensity for reflection h calculated from replicate data.

[b] Crystallographic R factor, $R_{cryst} = \Sigma||F_o| - |F_c||/\Sigma|F_o|$; $|F_o|$ and $|F_c|$ are the observed and calculated structure factor amplitudes, respectively, for those reflections not included in the R_{free} test set.

[c] Free R factor, $R_{free} = \Sigma||F_o| - |F_c||/\Sigma|F_o|$ for only those reflections included in the R_{free} test set.

[d] In asymmetric unit.

the aliphatic ether "tail" of the inhibitor makes no stabilizing interaction with this segment. This indicates that the 130's segment is so flexible that inhibitor binding cannot stabilize it in a discrete conformation. The resultant loss of 34 Å^2 of solvent-excluded surface area in the enzyme–inhibitor complex is most likely the key feature responsible for the 10-fold lower affinity of brinzolamide toward CAIV relative to CAII. Thus, the primary molecular determinant of weaker sulfonamide binding to isozyme IV relative to isozyme II is now established. This information may be useful in the design of even more effective, second-generation carbonic anhydrase inhibitors for use in glaucoma therapy.

Materials and methods

Crystallization

The hanging drop vapor diffusion method was used to crystallize murine CAIV, in which 3 μL of protein solution (4 mg/mL of murine CAIV in 15 mM Tris-HCl, pH 8.6) was equilibrated against 3 μL of 20% polyethylene glycol 4000, 100 mM Tris-sulfate, pH 7, at 4 °C. The biggest crystal appeared in two weeks and had approximate dimensions of 0.3 × 0.5 × 0.075 mm.

The murine CAIV–brinzolamide complex was cocrystallized using the same conditions as used for the native protein. The inhibitor was initially dissolved in DMSO with an inhibitor concentration of 100 mM. Subsequently, 1 μL of this stock solution was added to 100 μL of 4 mg/mL protein solution prior to setting up hanging drops crystallization trials. Crystals exhibited similar size and morphology to those of the native enzyme.

Crystals of native CAII were grown as described (Håkansson et al., 1992), and crystals of the CAII–brinzolamide complex were prepared as follows. Crystals were transferred into 4.0 M K_2HPO_4, pH 10, over a period of one day. After equilibrating overnight, these crystals were then crosslinked by slow transfer into 0.1% (vol/vol) glutaraldehyde in 4.0 M K_2HPO_4 to stabilize the crystal lattice. After 6–8 h, the crystals (yellow in color) were removed from the crosslinking solution, washed with 4.0 M K_2HPO_4 buffer, and allowed to sit in this buffer solution overnight. In order to prepare enzyme–inhibitor complexes, crystals were soaked in a 4.0 M K_2HPO_4 solution containing 4 mM inhibitor dissolved in DMSO such that the final concentration of DMSO in the solution was less than 10% (vol/vol) for three days.

Data collection

Diffraction data from crystals of murine CAIV were collected on an R-AXIS IIc image plate detector using Cu-Kα radiation (λ = 1.5418 Å) from a Rigaku RU-200HB rotating anode X-ray generator operating at 50 mV and 100 mA. Intensity data were processed with MOSFLM and CCP4 programs (Leslie, 1992; CCP4, 1994). Crystals diffracted X-rays to 2.8-Å resolution and belonged to space group $C222_1$, with unit cell parameters a = 53.5 Å, b = 85.2 Å, c = 121.9 Å. With one molecule in the asymmetric unit, the packing density, V_M = 2.3 Å^3/Da, indicated 47% solvent content (Matthews, 1968). Crystals of the CAIV–brinzolamide complex were isomorphous with those of native CAIV and likewise diffracted X-rays to 2.8-Å resolution. Crystals of the CAII–brinzolamide complex were isomorphous with those of the native enzyme (Håkansson et al., 1992) and diffracted X-rays to 2.25 Å resolution (Table 1).

Molecular replacement

The crystal structure of murine CAIV was solved by molecular replacement with AmoRe (Navaza, 1994). Using a truncated polyalanine model of CAIV as a search probe against 20.0–4.0-Å data, the cross-rotation search yielded the highest peak at 7.4σ with α = 153.6°, β = 42.4°, and γ = 74.2° (the second highest peak was at

4.6σ). Subsequently, the translation function calculation yielded an unambiguous solution with the highest peak at 6.5σ (the second highest peak was at 4.0σ). The crystallographic R-factor after rigid-body refinement was 0.428 using 20.0–2.8-Å resolution data. After iterative rounds of simulated annealing refinement with X-PLOR (Brünger et al., 1987) and model building, the final model of murine CAIV yielded a crystallographic R-factor of 0.182 (R_{free} = 0.267) with excellent stereochemistry (Table 1). Coordinates have been deposited in the Brookhaven Protein Data Bank with accession code 2ZNC.

CAII–brinzolamide and CAIV–brinzolamide complexes

Brinzolamide was fit into difference Fourier maps calculated against the native CAII and CAIV structures. Structures of the CAII–brinzolamide and CAIV–brinzolamide complexes were then refined with X-PLOR (Brünger et al., 1987) to final crystallographic R-factors of 0.144 and 0.191, respectively (Table 1).

Coordinates of the CAII–brinzolamide and CAIV–brinzolamide complexes have been deposited in the Brookhaven Protein Data Bank with accession codes 1A42 and 32NC, respectively.

Acknowledgments

We thank the NIH for grant GM45614 in support of this work. T.S. is the recipient of a Lynch Fellowship.

References

Bacon D, Anderson WP. 1988. A fast algorithm for rendering space-filling molecule pictures. *J Mol Graphics 6*:219–220.

Baird TT, Waheed A, Sly WS, Fierke CA. 1997. Catalysis and inhibition of human carbonic anhydrase IV. *Biochemistry 36*:2669–2678.

Baldwin JJ, Ponticello GS, Anderson PS, Christy ME, Murcko MA, Randall WC, Schwam H, Sugrue MF, Springer JP, Gautheron P, Grove J, Mallorga P, Viader M, McKeever BM, Navia MA. 1989. Thienothiopyran-2-sulfonamides: Novel topically active carbonic anhydrase inhibitors for the treatment of glaucoma. *J Med Chem 32*:2510–2513.

Ben-Tal N, Honig B, Peitzsch RM, Denisov G, McLaughlin S. 1996. Binding of small basic peptides to membranes containing acidic lipids: Theoretical models and experimental results. *Biophys J 71*:561–575.

Boriack-Sjodin PA, Heck RW, Laipis PJ, Silverman DN, Christianson DW. 1995. Structure determination of murine mitochondrial carbonic anhydrase V at 2.45 Å resolution: Implications for catalytic proton transfer and inhibitor design. *Proc Natl Acad Sci USA 92*:10949–10953.

Brechue WF, Kinne-Saffran E, Kinne RK, Marren TH. 1991. Localization and activity of renal carbonic anhydrase in alveolar-capillary barrier. *Biochim Biophys Acta 1066*:201–207.

Brown D, Zhu XL, Sly WS. 1990. Localization of membrane-associated carbonic anhydrase type IV in kidney epithelial cell. *Proc Natl Acad Sci 87*:7457–7461.

Brünger AT, Kuriyan J, Karplus M. 1987. Crystallographic R factor refinement by molecular dynamics. *Science 235*:458–460.

Camras CB, The Brinzolamide Primary Therapy Study Group. 1997. A triple-masked, primary therapy study of the efficacy and safety of BID and TID-dosed brinzolamide 1.0% compared to TID-dosed dorzolamide 2.0% and BID timolol 0.5%. *Invest Ophthalmol Vis Sci 38*:2606.

Cappalonga AM, Alexander RS, Christianson DW. 1992. Structural comparison of sulfodiimine and sulfonamide inhibitors in their complexes with zinc enzymes. *J Biol Chem 267*:19192–19197.

CCP4. 1994. Collaborative Computational Project, Number 4. *Acta Crystallogr D 50*:760–763.

Christianson DW, Fierke CA. 1996. Carbonic anhydrase: Evolution of the zinc binding site by nature and by design. *Acc Chem Res 29*:331–339.

Dean TR, May J, Chen HH, Kyba E, McLaughlin M, DeSantis L. 1997. Brinzolamide (AL-4862) suspension is a new topically active carbonic anhydrase inhibitor in the dutch-belted rabbit and cynomolgus monkey. *Invest Ophthalmol Vis Sci 38*:3786.

Effros RM, Mason G, Silverman P. 1981. Asymmetric distribution of carbonic anhydrase in alveolar-capillary barrier. *J Appl Physiol 51*:190–193.

Eriksson AE, Jones TA, Liljas A. 1986. Crystallographic studies of human carbonic anhydrase II (HCA II). In: Bertini I, Luchinat C, Maret W, Zeppezauer M, eds. *Zinc enzymes*. Boston: Birkhauser. pp 317–328.

Eriksson AE, Kylsten PM, Jones TA, Liljas A. 1988. Crystallographic studies of inhibitor binding sites in human carbonic anhydrase II: A pentacoordinate binding of SCN^- ion to the zinc at high pH. *Proteins Struct Funct Genet 4*:283–293.

Eriksson AE, Liljas A. 1993. Refined structure of bovine carbonic anhydrase III at 2.0 Å resolution. *Proteins Struct Funct Genet 16*:29–42.

Fleming RE, Crouch EC, Ruzicka CA, Sly WS. 1993. Pulmonary carbonic anhydrase IV: Developmental regulation and cell-specific expression in the capillary endothelium. *Am J Physiol 265*:L627–635.

Greer J, Erickson JW, Baldwin JJ, Varney MD. 1994. Application of the three-dimensional structures of protein target molecules in structure-based drug design. *J Med Chem 37*:1035–1054.

Hageman GS, Zhu XL, Waheed A, Sly WS. 1991. Localization of carbonic anhydrase IV in a specific capillary bed of the human eye. *Proc Natl Acad Sci USA 88*:2716–2720.

Håkansson K, Carlsson M, Svensson LA, Liljas A. 1992. Structure of native and apo carbonic anhydrase II and some of its anion–ligand complexes. *J Mol Biol 227*:1192–1204.

Honig B, Nicholls A. 1995. Classical electrostatics in biology and chemistry. *Science 268*:1144–1149.

Hurt JD, Tu C, Laipis PJ, Silverman DN. 1997. Catalytic properties of murine carbonic anhydrase IV. *J Biol Chem 272*:13512–13518

Kannan KK, Ramanadham M, Jones TA. 1984. Structure, refinement, and function of carbonic anhydrase isozymes: Refinement of human carbonic anhydrase I. In: Tashian RE, Hewett-Emmett D, eds. *Biology and chemistry of the carbonic anhydrases*. New York: New York Academy of Sciences. pp 49–60.

Kraulis PJ. 1991. MOLSCRIPT: A program to produce both detailed and schematic plots of protein structures. *J Appl Crystallogr 24*:946–950.

Leslie AGW. 1992. Recent changes to the MOSFLM package for processing film and image plate data. *CCP4 and ESF-EACMB Newsletter on Protein Crystallography 26*.

Liljas A, Kannan KK, Bergsten PC, Waara I, Fridborg K, Strandberg B, Carlbom U, Jarup L, Lovgren S, Petef M. 1972. Crystal structure of human carbonic anhydrase C. *Nature New Biol 235*:131–137.

Lucci MS, Tinker JP, Weiner IM, DuBose TD. 1983. Function of proximal tubule carbonic anhydrase defined by selective inhibition. *Am J Physiol 245*:F443–F449.

Mann T, Keilin D. 1940. Sulphanilamide as a specific inhibitor of carbonic anhydrase. *Nature 146*:164–165.

Maren TH. 1984. Biology and chemistry of the carbonic anhydrases. *Ann NY Acad Sci 429*:49–60.

Maren TH. 1987. Carbonic anhydrase: General perspectives and advances in glaucoma research. *Drug Dev Res 10*:255–276.

Maren TH, Wynns GC, Wistrand PJ. 1993. Chemical properties of carbonic anhydrase IV, the membrane-bound enzyme. *Mol Pharm 44*:901–905.

Matthews BW. 1968. Solvent content of protein crystals. *J Mol Biol 33*:491–497.

Merritt EA, Murphy MEP. 1994. Raster3D version-2.0—A program for photorealistic molecular graphics. *Acta Crystallogr D 50*:869–873.

Nair SK, Christianson DW. 1991. Unexpected pH-dependent conformation of His-64, the proton shuttle of carbonic anhydrase II. *J Am Chem Soc 113*:9455–9458.

Navaza J. 1994. AMoRe: An automated package for molecular replacement. *Acta Crystallogr A 50*:157–163.

Okuyama T, Sato S, Zhu XL, Waheed A, Sly WS. 1992. Human carbonic anhydrase IV: cDNA cloning, sequence comparison, and expression in COS cell membranes. *Proc Natl Acad Sci USA 89*:1315–1319.

Okuyama T, Waheed A, Kusumoto W, Zhu XL, Sly WS. 1995. Carbonic anhydrase IV: Role of removal of C-terminal domain in glycosylphosphatidylinositol anchoring and realization of enzyme activity. *Arch Biochem Biophys 320*:315–322.

Prugh JD, Hartman GD, Mallorga PJ, McKeever BM, Michelson SR, Murcko MA, Schwam H, Smith RL, Sondey JM, Springer JP, Sugrue MF. 1991. New isomeric classes of topically active ocular hypotensive carbonic anhydrase inhibitors: 5-Substituted thieno[2,3-*b*]thiophene-2-sulfonamides and 5-substituted thieno[3,2-*b*]thiophene-2-sulfonamides. *J Med Chem 34*:1805–1818.

Quigley HA. 1993. Open-angle glaucoma. *New Engl J Med 328*:1097–1106.

Shin DH, The Brinzolamide Adjunctive Therapy Group. 1997. A triple-masked, placebo controlled, adjunctive therapy study of the efficacy and safety of TID-dosed brinzolamide 1.0% compared to the TID-dosed placebo when used adjunctively to timolol 0.5%. *Invest Ophthalmol Vis Sci 38*:2605.

Silverman DN, Lindskog S. 1988. The catalytic mechanism for carbonic anhy-

drase: Implications of a rate-limiting protolysis of water. *Acc Chem Res 21*:30–36.

Sly WS, Hu PY. 1995. Human carbonic anhydrases and carbonic anhydrase deficiencies. *Annu Rev Biochem 64*:375–401.

Smith GM, Alexander RS, Christianson DW, McKeever BM, Ponticello GS, Springer JP, Randall WC, Baldwin JJ, Habecker CN. 1994. Positions of His-64 and a bound water in human carbonic anhydrase II upon binding three structurally related inhibitors. *Protein Sci 3*:118–125.

Stams T, Christianson DW. 1998. Structure–function relationships among the mammalian carbonic anhydrase isozymes. In: Chegwidden WR, Carter ND, Edwards YH, eds. *The carbonic anhydrases: New horizons*. Forthcoming.

Stams T, Nair SK, Okuyama T, Waheed A, Sly WS, Christianson DW. 1996. Crystal structure of the secretory form of membrane-associated human carbonic anhydrase IV at 2.8 Å resolution. *Proc Natl Acad Sci USA 93*:13589–13594.

Stewart R, The Brinzolamide Comfort Study Group. 1997. The ocular comfort of TID-dosed brinzolamide 1.0% compared to TID-dosed dorzolamide 2.0% in patients with primary open-angle glaucoma or ocular hypertension. *Invest Ophthalmol Vis Sci 38*:2603.

Tamai S, Waheed A, Cody LB, Sly WS. 1996. Gly-63 → Gln substitution adjacent to His-64 in rodent carbonic anhydrase IVs largely explains their reduced activity. *Proc Natl Acad Sci USA 93*:13647–13652.

Tielsch JM, Katz J, Sommer A, Quigley HA, Javitt JC. 1994. Family history and risk of primary open angle glaucoma. The Baltimore eye survey. *Arch Ophthalmol 112*:69–73.

Vidgren J, Liljas A, Walker NPC. 1990. Refined structure of the acetazolamide complex of human carbonic anhydrase II at 1.9 Å. *Int J Biol Macromol 12*:342–344.

Waheed A, Okuyama T, Heyduk T, Sly WS. 1996. Carbonic anhydrase IV: Purification of a secretory form of the recombinant human enzyme and identification of the positions and importance of its disulfide bonds. *Arch Biochem Biophys 333*:432–438.

Whitney PL, Briggle TV. 1982. Membrane-associated carbonic anhydrase purified from bovine lung. *J Biol Chem 257*:12056–12059.

Zhu XL, Sly WS. 1990. Carbonic anhydrase IV from human lung. *J Biol Chem 265*:8795–8801.